Journal of Colloid and Interface Science ••• (••••) •••–•••

Contents lists available at ScienceDirect

Journal of Colloid and Interface Science

www.elsevier.com/locate/jcis

Collective behavior during the exit of a wetting liquid through a network of channels

Charles N. Baroud [a,*], Xin C. Wang [a,b], Jean-Baptiste Masson [c,d,e]

[a] LadHyX and Department of Mechanics, Ecole Polytechnique, CNRS UMR 7646, 91128-F Palaiseau Cedex, France
[b] Massachusetts Institute of Technology, Cambridge, MA 02139, USA
[c] Laboratoire d'Optique et Biosciences, Ecole Polytechnique, 91128-F Palaiseau Cedex, France
[d] Laboratoire de Génétique des Génomes Bactériens, Institut Pasteur, CNRS URA 2171, 28 Rue du Docteur Roux, 75015 Paris, France
[e] Laboratoire de Génétique in Silico, Institut Pasteur, CNRS URA 2171, 28 Rue du Docteur Roux, 75015 Paris, France

ARTICLE INFO

Article history:
Received 20 November 2007
Accepted 18 June 2008

Keywords:
Imbibition
Porous network
Collective behavior
Microfluidic models

ABSTRACT

The exit of a wetting fluid from a thin microchannel into a sudden expansion is studied experimentally. In the case of the exit from a single channel, the advancing interface converges to a parabolic shape after an initial transient, in accordance with the lubrication limit analysis of a spreading drop. The experiments are then repeated for the exit from two parallel channels. At early times, the two exiting drops behave independently and display the same evolution as a single exiting droplet, while at late times we recover a single parabolic profile. The transition between the early and late states is due to the merging of the two drops, which is associated with a sudden increase in the flow rate. This is the signature of a collective effect which acts to redistribute the fluid spatially. Finally, the experiment is generalized to the case of seven parallel channels where a cascade of two-by-two mergings is observed, indicating that local interactions dominate the dynamics which lead to the global state of the system.

1. Introduction

The filling of a tube with a wetting fluid is a simple matter that rapidly becomes complex when the tube departs from the simplest circular cross-section, a result already observed by Jurin [1]. Although the physical ingredients are classical, the interaction between capillarity and geometry leads to surprising results which motivate current research. Indeed, the presence of angles and corners in the tube geometry, combined with the value of the contact angle which is given by material properties, modifies the curvature of the interface and can thus enhance or retard the entrance of the fluid into the tube [2,3]. The geometry can have such large effects that a threshold pressure can exist that blocks the exit of a liquid through an opening [4], while a convergent channel can produce movement of a plug with no external driving [5].

Several fields of science and engineering suffer (or benefit) from this complexity, particularly the flow of immiscible fluids through a porous medium. The economic impact of these flows, as well as the interest in the inherent physics of permeation, have motivated a large body of literature on the displacement of one fluid by another in the presence of a complex geometry, as discussed in the review article of Ref. [6]. In this context, microfluidics provides a useful approach to create model porous media with well controlled geometries by using photo-lithographic techniques, as demonstrated by the pioneering work of Lenormand [7,8]. More recently, the method of designing microchannels with a controlled complexity has been used in studies motivated by biomechanical [4,9,10], as well as technological questions [11,12].

In the systems modeling natural porous media, experimental work has often dealt with the flow of a wetting fluid into a network of obstacles [7,13]. Studies have typically concentrated on the global shape of the interface which displays a fingering instability with a fractal structure that extends over a large number of pores [14,15]. Furthermore, numerical pore-level models have also been developed to study the global behavior in a network of pores, using different shapes for the pores and for the channels [16].

Here we develop a microfluidic model to study the imbibition of a channel by a wetting liquid. We are particularly interested in the collective effects that occur when the single channel is replaced by two parallel channels, thus revisiting the doublet model of a porous medium described in [17]. We then generalize the approach to a large number of parallel pores. In contrast with other studies (e.g. [13]), we focus our attention on the initial exit from the channels and on the local shape of the interface, rather than on the global shape over a large number of pores. This approach

* Corresponding author.
E-mail addresses: baroud@ladhyx.polytechnique.fr (C.N. Baroud), jean-baptiste.masson@polytechnique.fr (J.-B. Masson).

0021-9797/$ – see front matter
doi:10.1016/j.jcis.2008.06.040

allows for detailed measurements of the interface shape as well as its temporal dynamics.

Moreover, by imposing that the resistance to flow through the channel is large, we may consider that the exit from a channel corresponds to the exit through a single pore, downstream of a large porous medium. In this case, the exit from two parallel channels is a model for studying the collective behavior at any two adjacent pores. In a random porous medium, the dynamics that occurs at the doublet level will be reproduced at many independent locations.

More generally, our study is also motivated by an analogy with the electromagnetic transmission through an array of sub-wavelength holes [18,19]. In these experiments a metallic screen pierced with sub-wavelength holes is able to transmit more energy than the total surface of holes should allow. Although the underlying process of the electromagnetic radiation is local and is caused by each hole, the transmission exhibits nonlocal characteristics such as resonance frequencies linked to the pattern of the metal screen. In the same way, the interactions of the wetting liquid with a small opening is local and influenced by the wetting properties, geometry, and pressure, but the total flow through a pattern of holes will show effects of global interactions. A carefully thought-out parallel between these two kinds of experiment may provide some insight into the mechanisms in the optics case. It may lead to the possibility of modeling some aspects of electron–photon interactions in a sub-wavelength hole array with a wetting formalism.

Below we begin by describing the experimental setup and the relevant pressure drops, followed by an analysis of the flow through a single pore in Section 3. In Section 4, we study the exit through two parallel channels and compare the results for early, intermediate, and late times with the single channel case. Finally, the two-channel results are generalized to a seven-channel case in Section 5, followed by a summary and conclusions.

2. Experimental protocol and pressure contributions

2.1. Experimental setup

The experiments were conducted in microfluidic channels of rectangular cross-section, made of polydimethylsiloxane (PDMS) by using soft lithography techniques, and bonded on a PDMS membrane which is spin-coated on a glass plate. The wetting conditions are therefore similar for all four channel walls.

As shown in Fig. 1, the geometry consists of a wide (1.2 mm width) inlet channel which leads to a long (1.6 mm) and thin (72 ± 3 μm) "impedance" channel. The latter opens into an exit channel, 2 mm wide, at right angles. The height is uniform at $h = 50$ μm for all the sections. The two and n-channel experiments use the same geometry but with the impedance channel replaced with parallel channels of the same width.

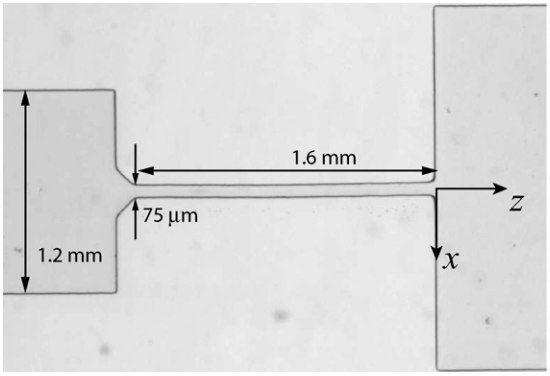

Fig. 1. Image of an empty channel. The fluid flows from left to right.

A constant driving pressure P_{dr} was applied using a water column of variable height, connected to a sealed oil vessel. The outlet of the exit channel was at atmospheric pressure. Different values of the driving pressure were obtained by varying the height of the water column, yielding P_{dr} in the range 100 to 2000 Pa (1–20 cm of water). The precision on the measurements of the meniscus height was 1 mm, giving a maximum error of 10% for the lowest pressure value.

The oil used in all experiments is pure paraffin oil with viscosity $\eta = 0.21 \pm 0.01$ Pa s and surface tension $\gamma \simeq 25 \times 10^{-3}$ N m^{-1}. The stationary contact angle of the oil on the PDMS was measured at about $\theta_0 \simeq 47^\circ \pm 2^\circ$. The flow of the oil into the channels was recorded using a digital camera, at a rate of 10 frames per second with a resolution of 900×500 pixels through a microscope at $2\times$ magnification, yielding images with 4 μm/pixel resolution. The data presented here were all extracted from image analysis codes written in our lab.

A typical experiment consisted of taking a new (clean) channel, setting the desired oil forcing pressure, then inserting the oil tube into the microchannel. A sequence of images was then taken of the advancing oil/air interface, all parameters being held constant. Taking advantage of the microfabrication techniques, many copies of the channels were fabricated in parallel on a single glass slide. This allowed many experiments to be run in sequence with clean channels but it also explains the slight variability between different experimental runs, namely in the impedance channel widths.

2.2. Relevant pressure drops

By taking a characteristic length scale $D = 100$ μm and typical velocity $U = 1$ mm s^{-1}, one obtains a Bond number of $Bo = \rho g D^2/\gamma \approx 3 \times 10^{-3}$ and a Reynolds number $Re = \rho U D/\eta \approx 4 \times 10^{-4}$, where $\rho = 850$ kg m^{-3} and $g = 9.81$ m s^{-2} are the density of the liquid and the acceleration of gravity, respectively. Therefore one may neglect both gravity and inertial effects, expecting the liquid dynamics to be governed by a visco-capillary regime. More importantly, the Capillary number ($Ca = \eta U/\gamma$) is also small at the exit of the impedance channel, typically ranging between $10^{-5} < Ca < 10^{-2}$.

In writing the pressure balance across the liquid exiting the impedance channel, two terms drive the advance of the oil while two terms resist the flow. The driving terms are (1) the imposed external pressure, P_{dr}, and (2) the wetting pressure $P_{cap}^{\perp}$. Indeed, the wetting effects force the fluid to invade the channel even in the absence of a driving pressure; the magnitude of $P_{cap}^{\perp}$ may be obtained from the oil/PDMS contact angle and the size of the gap between the upper and lower channel walls. Using our experimental conditions, we evaluate the underpressure inside the meniscus, which drives the wetting, at $2\gamma/h \cdot \cos(\theta_0) \simeq 700$ Pa.

The dominant term that resists the flow is the viscous pressure drop P_{pois}. Owing to the low Reynolds numbers, the different elements of the microchannels can be considered as resistors in series, or in parallel in the case of the multiple impedance channels. In each, a linear relation exists between the pressure drop and the flow rate Q, with the proportionality constant $\mathcal{R}$ depending on the channel geometry and on the oil viscosity. The pressure/flow rate relation is given by the classical Poiseuille law for rectangular channels [20], which can be written as

$$P_{pois} = \mathcal{R}Q = \frac{12\eta\ell}{wh^3[1 - 6\frac{h}{w}\sum_{n=0}^{\infty}\lambda_n^{-5}\tanh(\lambda_n w/h)]}Q, \qquad (1)$$

with h and w the channel height and width respectively and ℓ the length of liquid in the channel. The wavenumber, λ_n, may be written as

$$\lambda_n = \frac{(2n+1)\pi}{2}. \quad (2)$$

The resistance of the impedance channel is found to be $\mathcal{R} = 4.7 \times 10^{14}$ Pa s m^{-3}, while the resistance to flow in the inlet channel is found to be about an order of magnitude lower, at $\mathcal{R}_{\rm in} = 4.1 \times 10^{13}$. The oil flowing into the exit channel will also resist motion but that effect is negligible at early and intermediate times. Since the three resistors are in series, it is clear that the impedance channel will provide the limiting effect. Care must be taken, however, in the case of a large number of parallel channels (Section 5), where the total resistance of the impedance channels is divided by their number.

The final term which resists the invasion of the exit channel by the oil is the capillary jump due to the in-plane curvature, $P^{\parallel}_{\rm cap}$. This curvature takes on its maximum value as the liquid first exits the impedance channel and may be estimated by using a radius equal to the half-width of the channel, i.e. $r_{\rm min} = w/2$. The pressure jump at this maximum value would therefore be $\gamma/r_{\rm min} = 700$ Pa. This over-pressure rapidly decreases, however, as the curvature of the interface decreases.

In summary we calculate the oil flow rate by stating that $P_{\rm dr} + P^{\perp}_{\rm cap} - P^{\parallel}_{\rm cap} = (\mathcal{R} + \mathcal{R}_{\rm in})Q$. For a driving pressure of 800 Pa, we calculate $Q = 2.94 \times 10^{-12}$ m^3 s^{-1}. The measured steady state value of the flow is 3×10^{-12} m^3 s^{-1}, in good agreement with the model (Fig. 2). Below, we discuss details of the temporal evolution of the flow.

3. Flow through a single channel

Typical experimental results for the penetration of the oil in a single channel system are displayed in Fig. 2, where the interface shape and the total flow rate are shown as a function of time. The flow rate displays first a gradual decrease when the oil advances in the inlet channel, then a stronger decrease when it enters into the impedance channel. This is followed by a second decrease, shown in the circled region, as the oil exits the impedance channel. This last decrease is due to the strong in-plane curvature, which begins to resist the flow through the $P^{\parallel}_{\rm cap}$ term, and which is maximum at the exit of the channel. Finally, the flow rate reaches a constant value at late times, indicating that the in-plane curvature and the viscous dissipation in the exit channel are both negligible.

We shall mainly concentrate on the evolution of the shape of the oil/air interface as it exits the impedance channel. As seen in Fig. 2, the location of the interface can be observed with precision at every moment and we can measure the angle that the fluid makes with the sidewalls as a function of time. Initially, the fluid velocity at the contact point is relatively large and the contact angle deviates from its equilibrium value. However, the angle later decreases to its stationary value as the interface slows down. This is shown in Fig. 3, where the contact angle is plotted as a function of the contact point position, for the same data as in Fig. 2. We observe the contact angle going through a transition period, during which it takes a slightly increased value, but then settles to the equilibrium value for most of the traveled distance.

The shape of the interface is characterized by fitting it with a circle or a parabola, as shown in Fig. 4. The parabolic fits are plotted in Fig. 4a for four time steps after the drop exits the impedance channel. They reproduce well the interface shape, especially at late times, although they seem less precise at early times.

The quality of the fits can be measured by observing the evolution of the relative error as the interface advances and comparing the error in the parabolic vs circular fits. This is shown

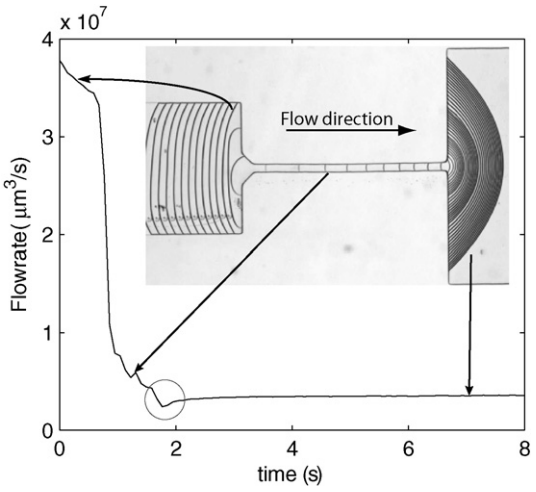

Fig. 2. Evolution of the flow rate as the fluid exits through a single channel. The driving pressure is $P_{\rm dr} = 785$ Pa. The image shows the location of the oil interface at a succession of times. For clarity, the time step used in the display is dilated as the liquid exits the channel, as seen by the apparent jumps in the interface position. The time step is $dt = 0.1$ s for the first period, $dt = 0.2$ s for the second, and $dt = 0.4$ s for the third.

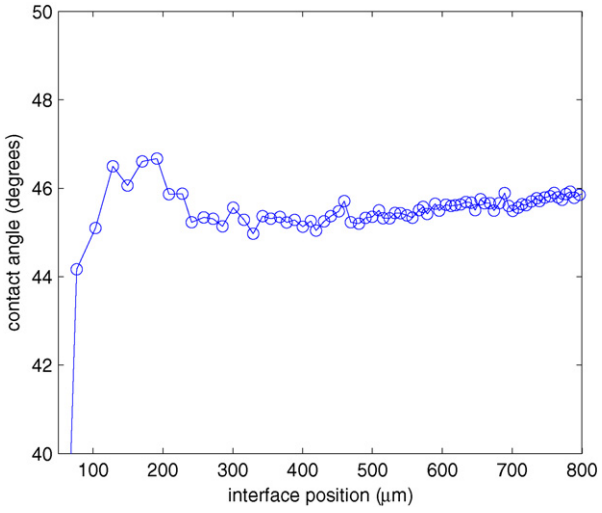

Fig. 3. Contact angle variation with interface position.

in Fig. 4b where the distance between the measured and fitted curves, summed over the whole interface and normalized by $\sum_{x_{\rm min}}^{x_{\rm max}} z(x)$, are plotted as a function of the interface width $dx(t)$. At early times, the circular fit better captures the interface shape, as shown by the smaller relative error. However, this trend is rapidly reversed and the interface becomes more parabolic in shape as it advances. The parabolic fit reaches the noise floor of our visualizations for $dx \simeq 1300$ μm and remains constant.

Although the circular fit is never very bad, it is useful to compare the shape of the interface with both fits in detail. This is done in Fig. 4c where the differences between the fitted and the real position are shown. Two details of the interface shape are poorly accounted for by the circular fit: First, the curvature of the interface does not seem constant, as seen by the systematic departures of the thick blue line from zero. Second, the value of the contact angle is poorly reproduced. Indeed, the curve shown in Fig. 4c is the best fitting circle; the best fitting circle which preserves the contact angle yields a poor fit. In contrast, the parabolic shape displays smaller and less systematic error in the shape, as well as agreeing well with the interface position at the edges.

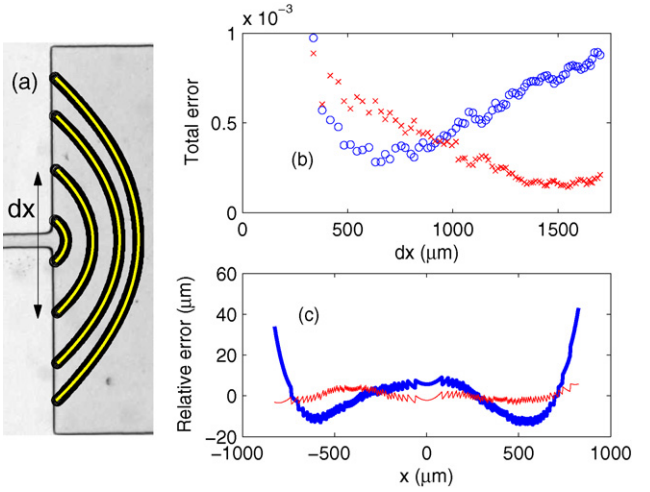

Fig. 4. (a) Interface (black thick line) and parabolic fit (yellow) at four different moments. (b) Normalized error for the circular (○) and parabolic (×) fits, as a function of dx. (c) Difference between the fitted and observed interface shapes for one image at late times: Circular (thick blue line) and parabolic (thin red line) fits. (For interpretation of the references to color in this figure legend, the reader is referred to the web version of this article.)

The parabolic profile of the interface has been predicted by Greenspan [21] for an axisymmetric drop spreading on a flat surface for cases where the derivative $\partial z/\partial x$ is small. Oron et al. [22] state that this is the "lubrication limit of a circle," meaning that it should provide a good approximation of the circle in the limit of small contact angles. Our measurements confirm that the shape taken by a spreading drop is indeed parabolic, even though we are in a confined quasi-two dimensional situation, with relatively large contact angles.

The interface is therefore a parabola, whose shape is determined by the contact angle between the oil and the PDMS, that we denote

$$z(x,t) = \kappa(t)\left[x^2 - x_m^2(t)\right], \tag{3}$$

where $\kappa(t)$ is not a function of spatial coordinates. Furthermore, the experiments show that the flow rate rapidly reaches a constant value after exiting the impedance channel, which implies that dx must increase as $t^{1/2}$ and that the curvature κ must scale as $\kappa \sim t^{-1/2}$. Both of these results are verified experimentally after the initial transient during which the interface changes shape.

Finally, the evolution of the apex (z_m) of the interface may be related to the evolution of the contact points at the sides ($\pm x_m$) as $z_m(t) = -\kappa(t)x_m^2(t)$. In addition, the contact angle between the PDMS and the oil is given by $\tan(\theta) = -2\kappa(t)x_m(t)$, which yields that

$$z_m(t) = \frac{\tan(\theta)}{2} x_m(t), \tag{4}$$

which is a linear function of $x_m(t)$ if the contact angle is constant.

4. Two parallel channels

Experiments performed in the previous section are repeated here with two parallel impedance channels, separated by a distance d which ranges from 200 to 500 μm. The goal is to characterize the differences in the flow rate and in the interface geometry between the flow with two channels and the flow with a single channel. The shape of the exiting interface is shown on the spatio-temporal plots in Fig. 5 for the three channel separations. We observe that two independent drops are formed initially at the exit of each channel and they grow in parallel. As the two interfaces begin to cover a distance comparable with the dimension d,

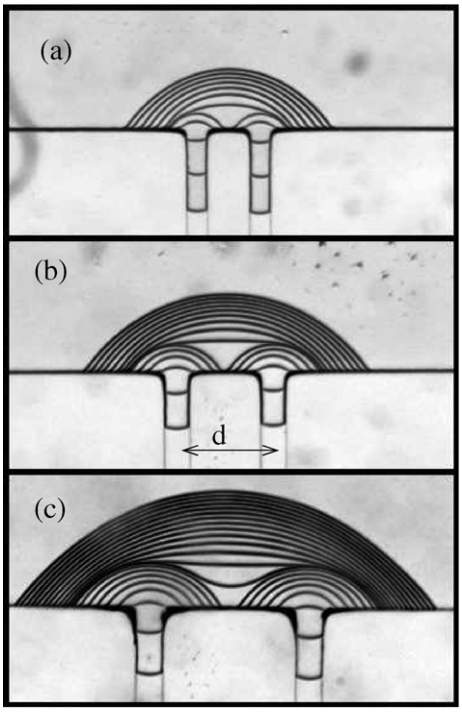

Fig. 5. The shape of the advancing interface for two impedance channels, separated by (a) 200, (b) 300, and (c) 500 μm. The flow here is from the bottom to the top. On all three figures, the driving pressure is 1200 Pa and the interface positions are separated by 0.1 s.

they start to interact, merging rapidly together when they meet. As one may expect, the shape of the interface relaxes to a parabola at late times, since the two channels look like a single (larger) channel if seen from far away.

The evolution of the flow rate with time is shown in Fig. 6. As in the single channel case, we observe a rapid decrease of the flow rate when the fluid enters the impedance channels, as well as an additional decrease when the interfaces reach the exit channel and change their curvature. This slowing down of the exiting drops acts to synchronize the two drops, in cases when they may have entered the channels at slightly different times. However, the merging of the two exiting drops strongly modifies dynamics by producing an overshoot in the flow rate, seen in the bump around $t = 3$ s. This increase can be understood by considering the negative curvature generated by the touching interfaces, which modifies the pressure balance by producing an additional capillary driving pressure. Finally, the flow converges toward a steady state value determined by the viscous resistance of two impedance channels in parallel.

The overshoot in the flow rate is associated with the transient during which the interface shape is out of equilibrium. The relaxation back to the late-time parabola may be explored by focusing our attention on the maximum position along the z direction, z_m, as a function of the width covered by the interface (dx). The evolution of $z_m(dx)$ is plotted in Fig. 7a for the single and double channel cases. In the single channel case, z_m smoothly increases after the exit from the impedance channel, approaching the straight line $z_m/\tan(\theta) = dx/4$, derived in Eq. (4). Here the mean steady state value of θ is used for all four experimental curves.

As expected, the curves for the two channels are related to the single channel case both initially and at long times: At the early times, the evolution for each exiting drop is identical to the single channel situation, as shown in Fig. 7b where the distance (d) between the inlet channels is subtracted from dx. We see that this leads to an exact superposition of z_m for all cases, indicating

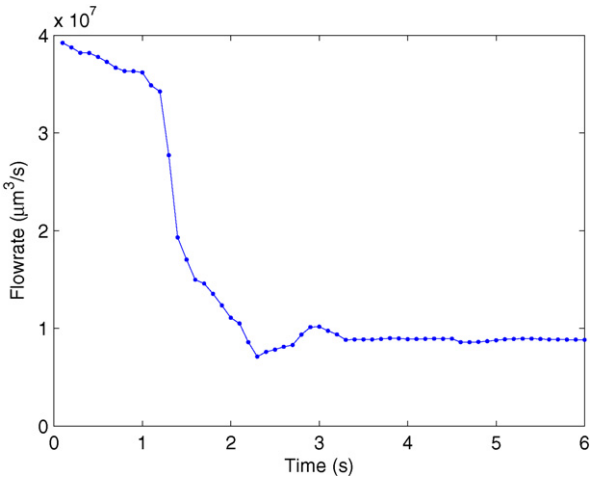

Fig. 6. Evolution of the total flow rate through the two-channel system, for $P_{dr} = 1200$ Pa and $d = 500$ μm.

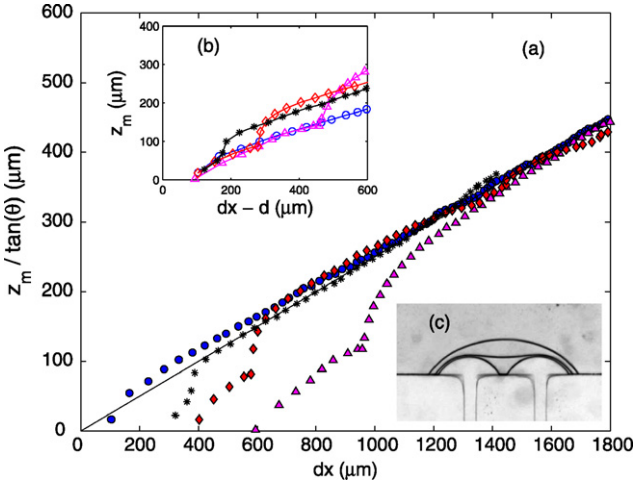

Fig. 7. (a) Evolution of the modified maximum position ($z_m/\tan(\theta)$) with respect to the width of the parabola (dx) for a single channel (○) and for two channels separated by 200 μm (∗), 300 μm (◇), and 500 μm (△). The straight line represents $dx/4$. (b) Same data with the interchannel distance (d) subtracted. (c) The interface before, during, and after the transition. See text for details.

that each drop initially exits as if it were isolated. At late times, the interface indeed relaxes to the parabolic shape since the dual-channel curves all relax to the $dx/4$ asymptote.

The transition between the two states occurs through the merging, which corresponds to the kink in the $z_m(dx)$ curves. Indeed, the merging produces a rapid movement of the interface in the z direction, while the velocity of the contact points is reduced significantly. This is also observed in Fig. 7c where the three important steps for the interface shape are displayed: just before merging, just after, and near the parabolic shape. The passage from just before to just after is very rapid [23] and is not resolved by our imaging frame rate. The dynamics during this phase, corresponding to a large transient value of the capillary number, is driven by the large local curvature which yields correspondingly large flux locally. However, this transient only lasts until the curvature decreases, since the viscous diffusion time is very short ($\tau_{visc} = h^2\rho/\eta \simeq 10$ μs) and viscosity rapidly dissipates any large velocities that may appear.

This fast transient is followed by the rate limiting step which is estimated by writing an equilibrium between the pressure imbalance due to the curvature variations and the viscous resistance. Indeed, the interface quickly reaches a situation where it is curved

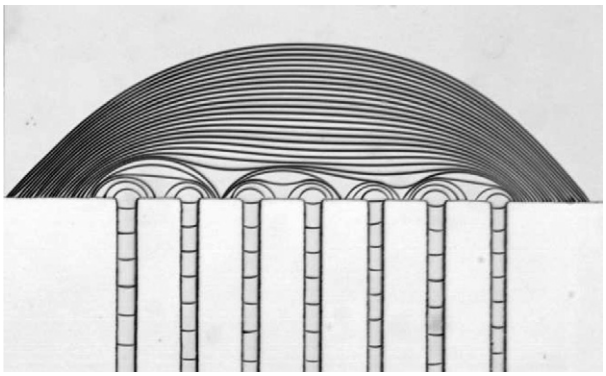

Fig. 8. Advance of an interface through seven independent channels. The time separating each line is 0.1 s.

near the contact points and flat in the central region, which leads to a redistribution of the fluid due to the unequilibrated Laplace pressure. Using the parabolic approximation of the interface shape, we may therefore write

$$\Delta P \approx \frac{\gamma}{\kappa} \approx \frac{\gamma \tan(\theta)}{d}. \tag{5}$$

This driving pressure is balanced by the viscous pressure term, which may be approximated by the Hele–Shaw formula as

$$\Delta P \approx \frac{12\eta}{h^2} LV, \tag{6}$$

where L is a characteristic distance traveled by the fluid and V a characteristic velocity of the interface. Geometric considerations give $L \approx d/2$ and $V \approx L/T$ with T the time to go from one state to the other. Equating Eqs. (5) and (6) yields

$$T \approx \frac{3\eta d^3}{\gamma \tan(\theta) h^2}, \tag{7}$$

which leads to $T_{200} \simeq 0.1$ s, $T_{300} \simeq 0.3$ s, and $T_{500} \simeq 1.3$ s for $d = 200$, 300 and 500 μm, respectively. These values are consistent with the times observed in Fig. 7a which can be obtained by counting the points that separate the kink from the asymptotic curve and recalling that they are separated by $dt = 0.1$ s.

5. *n*-Channels

The results from the two-channel experiments can be generalized to a large number of parallel channels. For this, the experiments above were repeated using seven parallel channels, separated by $d = 200$ μm, using different forcing pressures. As in the doublet case, the initial exit of the interface reproduced a single channel exit and the late times displayed the parabolic shape. Interestingly however, most merging events that we recorded involved only two adjacent drops while less than 10% involved three (see Fig. 8). We never observed mergings that simultaneously involved a large number of channel exits. The newly formed interfaces merged again by groups of two and so on.

The evolution of the interface after each merging event is similar to the evolution in the doublet case: The curvature is high near the edges while the interface is flat between the two channels. As seen in the curves of Fig. 7, this state redirects the fluid into the center of the newly merged interface, temporarily preventing the drop from spreading laterally and by the same token preventing further mergings from taking place. This explains why the two channel merging is the most probable dynamics. Its main consequence is that only local interactions act on the flow at early times, the interactions remaining local until there is only one continuous interface. There are therefore no delocalized interactions

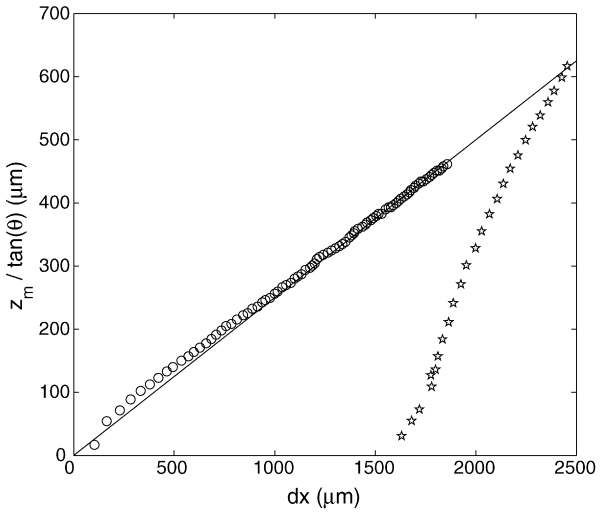

Fig. 9. Evolution of z_m as a function of dx for the single channel case as before (○) and for the seven channel case (⋆). The straight line represents $dx/4$.

propagating on the scale of several channels, thus justifying the study of the two-channel case as the basic ingredient that leads to the large scale behavior.

At the end of the merging cascade, the curvature is again high near the two extreme channels and almost nil on the rest of the interface. Given the large separation between the end channels, the interface relaxes to its parabolic shape over a long period, given by the total size of the network. During this time, the lateral velocity of the fluid is slow and the flux is largely directed towards the central region (Fig. 9). Note that an important consequence of this flow regime is that the seven channels are not equivalent and cannot be treated as resistors in parallel, since the flux is unevenly distributed among them. In this way, the strictly local interactions of the binary mergings have a global impact on the flow distribution and on the total resistance of the network. Finally the interface converges toward the parabolic shape observed previously. This situation resembles the parabolic solution predicted for a drop spreading and imbibing a porous medium [24], although the flux through the holes representing the porous medium is reversed in this case.

6. Summary

In summary, the study of the flow of a wetting liquid through a single control channel was studied. While the pressure balance yielded a good estimate for the flow rate, the interface was found to depart significantly from circularity and to take a parabolic shape. This result is in agreement with the lubrication theory analysis [21], although our contact angles significantly depart from zero.

The results for the single channel were found to give an excellent basis for the short and long term behavior of fluid going through doublets or multiple channels. The transition between the early and late times was dominated by the capillary phenomena of the merging and involved a temporary increase in the flow rate, due to an additional capillary underpressure term, during a time which is given by a balance between the underpressure and the viscous drag. This signature of collective behavior operated on a two-by-two basis, even in the case of a large number of parallel channels.

The collective behavior in the advance of a fluid into a complex geometry has been a subject of interest in many areas of science and technology for a long time. The capabilities offered by microfluidics and image analysis offer a new way to model these questions. We have considered in this article the simplest geometry of flow exiting a single control channel, a doublet, and seven identical parallel channels. This work can now be extended to more complex geometries involving for example sub-groupings of channels or channels with nonparallel walls.

Acknowledgments

XCW's internship was funded in part by the Direction des Relations Extérieures of Ecole Polytechnique and in part by the MIT-France program.

References

[1] J. Jurin, Philos. Trans. R. Soc. 30 (1717) 739–747.
[2] J. Bico, D. Quéré, J. Colloid Interface Sci. 247 (1) (2002) 162–166.
[3] V.S. Ajaev, G.M. Homsy, Annu. Rev. Fluid Mech. 38 (1) (2006) 277–307.
[4] C.P. Ody, C.N. Baroud, E. de Langre, J. Colloid Interface Sci. 308 (2007) 231–238.
[5] A.A. Darhuber, S.M. Troian, Annu. Rev. Fluid Mech. 37 (2005) 425–455.
[6] M. Alava, M. Dube, M. Rost, Adv. Phys. 53 (2) (2004) 83–175.
[7] R. Lenormand, C. Zarcone, A. Sarr, J. Fluid Mech. 135 (1983) 337–353.
[8] R. Lenormand, C. Zarcone, Phys. Rev. Lett. 54 (May 1985) 2226–2229.
[9] C.N. Baroud, S. Tsikata, M. Heil, J. Fluid Mech. 546 (2006) 285–294.
[10] A.J. Calderón, Y.S. Heo, D. Huh, N. Futai, S. Takayama, J.B. Fowlkes, J.L. Bull, Appl. Phys. Lett. 89 (2006) 244103.
[11] D.R. Link, S.L. Anna, D.A. Weitz, H.A. Stone, Phys. Rev. Lett. 92 (5) (2004) 054503.
[12] M. Zimmermann, H. Schmid, P. Hunziker, E. Delamarche, Lab Chip 7 (2007) 119–125.
[13] V. Berejnov, N. Djilali, D. Sinton, Lab Chip 8 (2008) 689–693.
[14] A. Dougherty, N. Carle, Phys. Rev. E 58 (1998) 2889–2893.
[15] G. Lovoll, Y. Meheust, R. Toussaint, J. Schmittbuhl, K.J. Maloy, Phys. Rev. E 70 (2) (2004) 026301.
[16] M.J. Blunt, H. Scher, Phys. Rev. E 52 (6) (1995) 6387–6403.
[17] F.A.L. Dullien, Porous Media: Fluid Transport and Pore Structure, Academic Press, 1979.
[18] J.B. Masson, G. Gallot, Phys. Rev. B 73 (12) (2006) 121401.
[19] J.-B. Masson, G. Gallot, ArXiv: 0714.3945v1, 2007.
[20] F.M. White, Viscous Fluid Flow, McGraw–Hill, 1991.
[21] H.P. Greenspan, J. Fluid Mech. 84 (1978) 125–143.
[22] A. Oron, S.H. Davis, S.G. Bankoff, Rev. Mod. Phys. 69 (3) (1997) 931–980.
[23] J. Eggers, J.R. Lister, H.A. Stone, J. Fluid Mech. 401 (1999) 293–310.
[24] S.H. Davis, L.M. Hocking, Phys. Fluids 11 (1) (1999) 48–57.